Optical Engineering

SPIEDigitalLibrary.org/oe

Development and performance of a filter radiometer monitor system for integrating sphere sources

Leibo Ding
Matthew G. Kowalewski
John W. Cooper
Gilbert R. Smith
Robert A. Barnes
Eugene Waluschka
James J. Butler

Optical Engineering 50(11), 113603 (November 2011)

Development and performance of a filter radiometer monitor system for integrating sphere sources

Leibo Ding
SigmaSpace Corporation
Lanham, Maryland 20706

Matthew G. Kowalewski
Universities Space Research Organization
Columbia, Maryland 21044

John W. Cooper
Gilbert R. Smith
SigmaSpace Corporation
Lanham, Maryland 20706

Robert A. Barnes
Science Applications International Corporation
Beltsville, Maryland 20705

Eugene Waluschka
James J. Butler
NASA Goddard Space Flight Center
Greenbelt, Maryland 20771

Abstract. The NASA Goddard Space Flight Center (GSFC) Radiometric Calibration Laboratory (RCL) maintains several large integrating sphere sources covering the visible to the shortwave infrared wavelength range. Two critical, functional requirements of an integrating sphere source are short- and long-term operational stability and repeatability. Monitoring the source is essential in determining the origin of systemic errors, thus increasing confidence in source performance and quantifying repeatability. If monitor data falls outside the established parameters, this could be an indication that the source requires maintenance or recalibration against the National Institute of Science and Technology irradiance standard. The GSFC RCL has developed a Filter Radiometer Monitoring System (FRMS) to continuously monitor the performance of its integrating sphere calibration sources in the 400 to 2400 nm region. Sphere output change mechanisms include lamp aging, coating (e.g., $BaSO_4$) deterioration, and ambient water vapor level. The FRMS wavelength bands are selected to quantify changes caused by these mechanisms. The FRMS design and operation are presented, as well as data from monitoring four of the RCL's integrating sphere sources. [DOI: 10.1117/1.3646532]

Subject terms: integrating sphere; calibration; stability; radiometer.

Paper 110708PR received Jun. 22, 2011; revised manuscript received Sep. 14, 2011; accepted for publication Sep. 15, 2011; published online Nov. 11, 2011.

1 Introduction

Two critical requirements of any optical calibration source are short- and long-term operational stability and repeatability. Without continuous monitoring of the source, short-term source instabilities may not be noticed and could possibly be incorrectly attributed to instabilities or transients in the instrument being calibrated. Also, long-term source instabilities may never be detected until the source output diverges grossly, making repeatability difficult to establish.

The degradation of sphere radiant output is wavelength dependent. Commercial sphere source output monitoring devices usually consist of a single silicon detector sometimes equipped with a broadband photopic filter mounted at a port on the sphere. As a result of the broadband wavelength response of the silicon detector, only gross sphere output degradation or variability is detected. These monitoring devices are insufficient to detect the wavelength selective degradation that would affect the individual narrow band wavelengths of radiometers being calibrated by the source. Examples of the importance of monitoring short- and long-term stability and repeatability can be found in the historical applications of integrating spheres in the calibration of satellite Earth remote sensing instruments.[1–5] For many of these applications, the calibration of the integrating sphere is performed well before being used in the calibration of the satellite instrument. It is erroneous to assume that the integrating sphere output is unchanged between the times of its calibration and its use. For these cases, in order to realize radiance calibration uncertainties of 3% to 5% ($k = 1$) typical of NASA's Earth Observing System (EOS) satellite instruments operating from 400 to 2500 nm, the output of integrating sphere sources must be continuously monitored using stable radiometers operating at or across the satellite instrument wavelengths.

The Goddard Space Flight Center (GSFC) Radiometric Calibration Laboratory (RCL) maintains and operates a suite of integrating sphere sources capable of meeting the radiance and irradiance calibration requirements of satellite instruments viewing a dark ocean to bright clouds. The integrity of the GSFC RCL integrating sphere sources is maintained with National Institute of Science and Technology (NIST) traceable calibrations. Sphere source output radiance is slightly variable and unstable as a function of the type and condition of the internal reflectance surface, the aging characteristics of the internal lamps, and sphere ambient relative humidity and temperature. As a result, there exists a need to continuously monitor the stability of the sphere source output over their wavelength operating range of 400 to 2400 nm. The production of high quality, accurate sphere source data requires that this variability be monitored and, if necessary, used to apply a correction factor to the data. The GSFC RCL Filter Radiometer Monitoring System (FRMS),[6] whose development and performance are now fully described in this paper, is an optically simple yet versatile 11 band filter radiometer used in the RCL to monitor sphere stability and repeatability. In combination with additional instrumentation, the FRMS is also shown to be able to measure sphere uniformity and to characterize the polarization properties of sources and optics.

2 FRMS Description

A dedicated, optically simplistic, electronically stable detector and optical filter monitoring system best serves the need

0091-3286/2011/$25.00 © 2011 SPIE

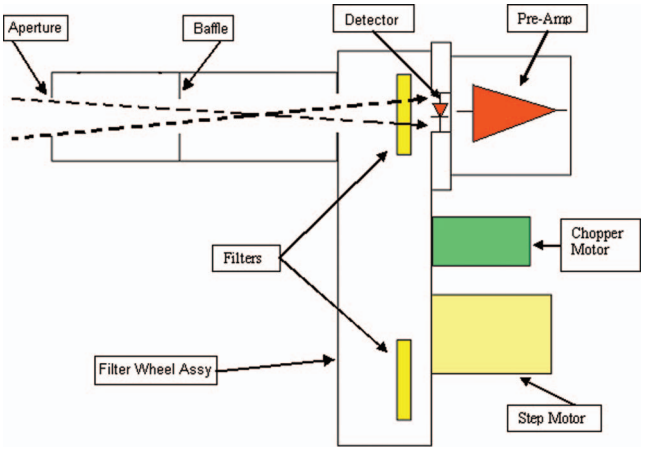

Fig. 1 A block diagram of the FRMS.

to document the degradation and variability of the sphere output. The GSFC integrating sphere source FRMS is such a system and provides time line data of the sphere output stability and variability. A greater confidence in the integrity of the sphere output will thereby be maintained through use of the FRMS. The FRMS is a filter wheel radiometer and is a computer controlled, software operated unit. A block diagram of the FRMS is shown in Fig. 1. The optical input of the FRMS is a Gershen tube with apertures to define the full field of view (FOV). The FOV is defined by the incident light (i.e., dashed lines) shown in Fig. 1. The FRMS sphere source data are assets in determining the origin of systematic errors, thus increasing confidence in sphere source performance and in quantifying source repeatability. If monitor data falls outside established parameters, this is an indication that the source may require maintenance or recalibration against the standard. Several FRMS optical filter wavelength bands have been selected to be in those areas of scientific interest that are sensitive to the mechanisms of common degradation of the sphere output.

The heat from the lamps of sphere sources naturally causes the sphere to be elevated in temperature to the extent that this is detrimental to the performance and stability of the FRMS detector, optical assembly, and electronics. Therefore, directly mounting the FRMS to a small aperture on the sphere source is impractical at this time. The FRMS must be thermally isolated from the sphere. Thermal isolation from the sphere can be realized by placing a fiber optic bundle or a light pipe between the sphere and the FRMS entrance aperture. These methods are currently under investigation. In lieu of this, data have been gathered with the FRMS placed on a table, viewing the main aperture of the sphere at a distance of 50 cm (Fig. 2). The FRMS has been tested and characterized and the results are presented.

3 Detector Heads

An ultraviolet (UV) enhanced silicon (Si) detector is used for the FRMS in the wavelength range of 400 to 1100 nm. A second FRMS employs an extended indium gallium arsenide (InGaAs) detector and is used for the wavelength range of 1100 to 2400 nm. Also, two additional detectors are available for use with the FRMS: a two-element "sandwich" detector composed of an Si element and an InGaAs element to cover the spectral range of 320 to 2570 nm and a Ge detector for the spectral range of 800 to 1800 nm.

The two-element detector is a hybrid sandwich-style detector containing an infrared-transmitting Si photodiode mounted over an InGaAs PIN photodiode configured along the same optical axis. The benefits of using the two-element detector are the wide spectral response range and the single optical axis configuration for both detectors. The drawbacks are lower sensitivities and a smaller active area for the InGaAs detector, making it an undesirable choice for the applications with a chopper. Table 1 is a data sheet for these detectors. A transimpedance amplifier (i.e., current-to-voltage converter) is used for the pre-amp. The selection of the operational amplifier (OA) is based on low noise, low drift, low bias (i.e., voltage and current), low input capacitance, high gain, and high resistance. To reduce the noise, "the simpler is better" principle is applied for the pre-amp: the detector is set as close as possible to the input of the pre-amp; and there is no selection switch (e.g., sensitivity selection, bias cancellation, detector type selection). The pre-amp contains an OA, a precision resistor, and a tiny-value capacitor for frequency compensation. Each detector has a dedicated pre-amp with different resistor and capacitor. The voltage signal from the OA is directly sent to a digital multimeter HP 3458A without any modification. A second-stage amplifier can be used, but

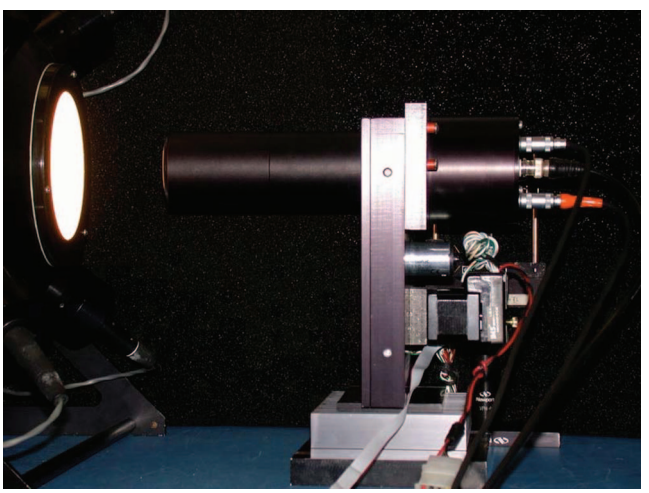

Fig. 2 The FRMS monitoring an integrating sphere source.

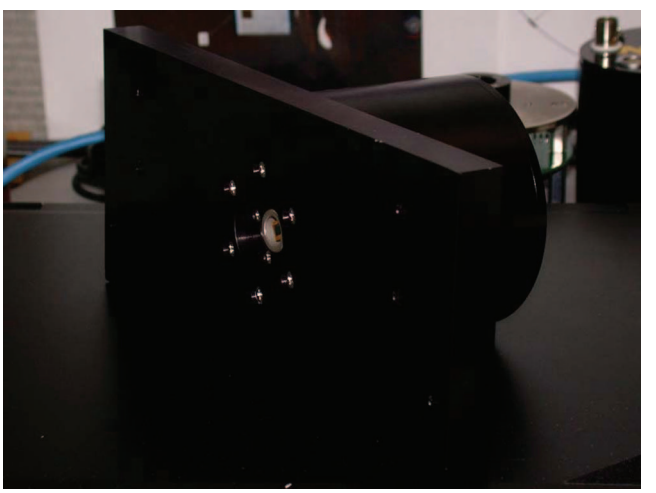

Fig. 3 The FRMS detector head.

Table 1 Detectors used in the FRMS.

Detector element		Cooling	Active area size (mm)	Spectral response range (nm)	Sensitivity @ λ_P[d] (A/W)	Dark current	Shunt resistance R_{sh}	NEP @λ_P[d] (W/Hz$^{1/2}$)
Si		One-stage TE-cooled (−10°C)	2.4×2.4	190 – 1100	0.5	10 pA[a]	1 GΩ[a]	8.1×10^{-15} [b]
Extended-InGaAs		Two-stage TE-cooled (−20°C)	Ø3	1200 – 2570	1.3	7.5 μA[c]	6 KΩ[a]	1.8×10^{-12} [b]
Two-element detector	Si	One-stage TE-cooled (−10°C)	2.4×2.4	320 –1670	0.45	50 pA[a]	200 MΩ[a]	
	InGaAs	One-stage TE-cooled (−10°C)	Ø1		0.55	70 pA[c]	1.5 GΩ[a]	
Extended two-element Detector	Si	One-stage TE-cooled (−10°C)	2.4×2.4	320 – 2570	0.45	50 pA[a]	200 MΩ[a]	
	InGaAs	One-stage TE-cooled (−10°C)	Ø1		0.60	1.5 μA[c]	30 KΩ[a]	
Ge		Two-stage TE-cooled (−20°C)	Ø5	800 – 1800	0.8	30 nA[a]	330 KΩ[a]	3.0×10^{-13} [b]

[a]25°C, $V_R = 10$ mV.
[b]25°C, $V_R = 0$ V.
[c]25°C, $V_R = 1$ V.
[d]λ_P = Peak sensitivity wavelength.

it is not necessary in this application. The detector and the pre-amp are mounted in a metal cylinder-shaped container as shown in Fig. 3.

4 Filters and Filter Wheel

One opaque blocking element and 11 bandpass filters of 2.54-cm diameter were installed for the FRMS initial testing and characterization. The filter center wavelengths/bandwidths in nanometers are as follows: 410/10, 440/10, 460/10, 640/10, 840/10, 1050/15, 1240/20, 1380/20, 1640/20, 2130/30, and 2210/25. All filters are stock items. Filter selection is critical and the initial filter bands were selected to measure and bracket spectral scientific regions of interest. The 840 and 1050 nm bands are used to monitor the source output spectral peaks; the 1240, 1380, and 1640 nm bands bracket the first significant water absorption band; while 2130 and 2210 nm bands are used to monitor the infrared spectral characteristics of the sources. Past experience in operating quartz tungsten halogen lamps of the type used as RCL sources suggests that lamp degradation is most noticeable in the UV region and this drove selection of the 410, 440, and 460 nm bands to monitor lamp degradation. Also, the 410 and 440 nm bands are widely used by other standard transfer radiometers, such as the Sea-viewing Wide Field-of-view Sensor (SeaWiFS) transfer radiometer (SXR) and the Earth Observing System (EOC) Visible Transfer Radiometer (VXR) and as Moderate Resolution Imaging Spectroradiometer (MODIS) bands. Note that the initial filters are exchangeable with other bandpass filters according to applications. Figure 4 shows the 12-position rotating filter wheel.

Fig. 4 The FRMS optical filter wheel.

5 FRMS Electronic Noise Level and Stability

The FRMS electronic noise includes the dark noise from the detector photodiode and the operational amplifier noise and offset.[7] To measure this noise, the opaque blocking element is used to cover the detector's input window, and the output from the operational amplifier (i.e., the dark signal) was recorded. The stability of the dark signal is a direct indication of the stability of the detector head, that is, the combination of the detector and pre-amp.

The dark signal is measured along with other filters' signals and was used as the reference signal subtracted from the optical filter signals. Figure 5 shows a typical dark signal plot. The two-element detector, the K3413-09 thermo-electrically cooled Si + InGaAs detector, was used to acquire these data using the RCL 1/GSFC 1.83 m diameter large integrating sphere called "Hardy." Details on this and other integrating spheres used in this study are provided in Sec. 6. In this measurement of dark signal, the sphere was turned on with all

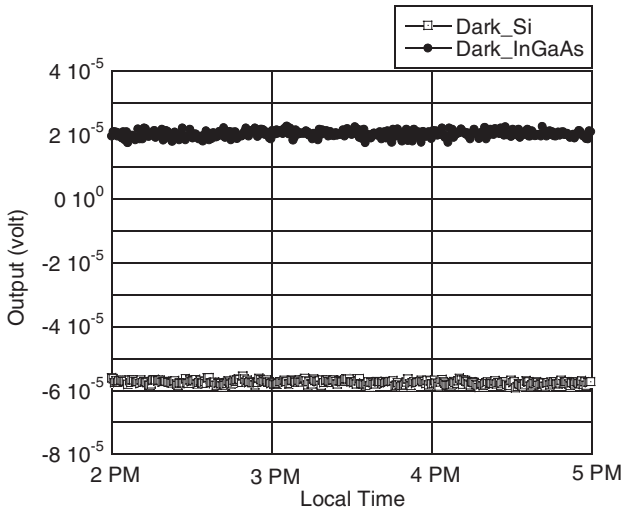

Fig. 5 FRMS dark signals for the thermo-electrically cooled silicon + InGaAs detector.

16 lamps, then dropped to the 12 lamp level, and finally was turned off. During this period, the ambient temperature increased from 23.9°C to 36.7°C; but the dark signals remained stable.

6 Sphere Response Stability Measurements

Five integrating sphere sources were used to evaluate and characterize the FRMS. They are listed below:

- 1/GSFC 1.83 m diameter integrating sphere, dubbed "Hardy," with a barium sulfate ($BaSO_4$) interior coating and a 25.4-cm diameter exit aperture. This sphere is equipped with 16 baffled 200 W quartz tungsten halogen lamps.
- 2/GSFC 91.4 cm diameter polytetrafluoroethylene (PTFE) integrating sphere, dubbed "Slick," lined with Spectralon^{TM} and a 25.4-cm diameter exit aperture. This sphere is equipped with 16 unbaffled 45 W quartz tungsten halogen lamps.
- 3/GSFC 50.8-cm diameter PTFE integrating sphere, dubbed "Venti," lined with Zenith^{TM} coating and a 20.3-cm diameter exit aperture. This sphere is equipped with 4 quartz tungsten halogen lamps: two 150 W, one 300 W, and one 75 W with an attenuator.
- 4/GSFC 101.6-cm diameter PTFE integrating sphere, dubbed "Grande," lined with Zenith^{TM} coating and a 25.4-cm diameter exit aperture. This sphere is equipped with 8 baffled 300 W quartz tungsten halogen lamps and one 150 W quartz tungsten halogen lamp with a variable attenuator.
- 5/NASA Ames Research Center (ARC) 15.2-cm diameter radiance standard OL-455 with a $BaSO_4$ interior coating and a 3.8-cm diameter exit aperture dubbed "ARS455." This sphere is equipped with a single 150 W quartz tungsten halogen lamp.

Other instruments used to characterize the FRMS include:

- The Shuttle Solar Backscatter Ultraviolet (SSBUV) instrument: The SSBUV is a refurbished Solar Backscatter Ultraviolet/2 instrument of the type flown on the NOAA Polar Orbiting Environmental Satellites. This instrument was flown 8 times on the Space Shuttle between 1989 and 1996. The instrument is a scanning double Ebert–Fastie holographic spectrometer with 1.1 nm bandpass operating from 240 to 405 nm.
- An Avantes Spectrometer, AvaSpec-2048-USB2 with UA-300 lines/mm grating, 50 μm slit, 2048 pixel CCD detector, 16 bit ADC, a spectral range of 200 to 1100 nm, and a spectral resolution of 2.4 nm.
- Two analytical spectral devices (ASD) FieldSpec3 Full Range spectrometers with spectral ranges of 350 to 2500 nm and a FWHM spectral resolution of 3 nm from 350 to 1000 and 10 nm from1000 to 2500 nm.

6.1 *Short-Term Stability Measurements*

Three of the GSFC integrating spheres were monitored by the FRMS and the results are plotted in Figs. 6–8. For each measurement, the data were normalized to 100% after the required sphere warm up time.

In Fig. 6, the two upper plots, (a) and (b), were from measurements taken on October 16, 2008. At the same time, an ASD was used to make a comparison with the FRMS and the results are shown in Fig. 6(c). The results show reasonable agreement with each other. Figure 6(d) shows the results from the FRMS equipped with an extended InGaAs detector on another day.

In Fig. 7 (i.e., 2/GSFC 91.4-cm diameter Slick), the two upper plots, (a) and (b), show two measurements from the FRMS Si and Ge detectors. At the same time, the Avantes Spectrometer was used to cross calibrate the FRMS and its results are plotted as Figure 7(c). The cross calibration also shows consistency between the FRMS and the Avantes Spectrometer. Figure 7(d) shows the results from the FRMS equipped with an extended InGaAs detector on another day.

In Fig. 8 (i.e., 3/GSFC 50.8-cm diameter sphere Venti), the plots show the stability measurement results from the FRMS equipped with Si and Ge detectors.

Table 2 shows the calculated noise equivalent radiance (NER) using the 2/GSFC 91.4-cm diameter Slick integrating sphere with all lamps illuminated. The measurement uncertainty and the related NER associated with the FRMS are determined by observing the signal level and the maximum amplitude of the dark signal for each channel. The signal level is related to radiance level. The maximum amplitude of the dark signal is obtained by observing the dark signal plots as shown in Fig. 5. The maximum amplitude of the dark signals associated with the Si, Ge, and extended InGaAs detectors are 4, 40, and 6 μV, respectively. The FRMS uncertainty is calculated as: maximum amplitude/signal level. The NER is obtained by multiplying the uncertainty by the radiance level.

6.2 *Measurement Comparison with SSBUV*

On February 7, 2008, a measurement comparison between the FRMS and the SSBUV was performed at the GSFC Code 613.3 Radiometric Calibration and Development Laboratory. The 5/NASA ARC 15.2-cm diameter ARS455 sphere was used as the radiance standard. Since there was no overlapping spectral range between these two instruments, two filters,

360/10 and 380/10, were selected to replace two of the initial optical bandpass filters in the FRMS. The data at 360 and 380 nm were compared between the FRMS and the SSBUV; and results are plotted in Fig. 9. For each measurement, the data were normalized to 100% after the required sphere warm up time.

6.3 *Long-Term Stability Measurements*

One of the capabilities of the FRMS is to monitor a sphere's long-term stability. Since the FRMS design and operational mode have not been completely finalized, a long-term database has not been acquired to validate this function. Once the FRMS is finalized, data will be acquired every month or after every 100 h of usage and the results will be plotted to show the trends. These data will provide insight into the degradation and variation of sphere lamps and interior coatings. Sphere data acquired over several days with identical warm-up times are shown in Fig. 10. The data taken on October 17, 2009 are used as a reference; data taken after that date are compared to that reference. The determination of long-term stability requires long data accumulation times. Therefore, these plots are provided for demonstration only.

Further examination of the day-to-day data in Fig. 10 revealed a significant change in radiance of 0.5% to 1%. We have attributed the cause of this additional uncertainty to be the relative instability of the lamp power supplies. Vendor data indicates power supply current accuracy to better than 12 mA (i.e., 0.17% in current). Our laboratory measurements indicate that a change of 1.5 mA in power supply current (i.e., 0.025%) will cause a change of 0.1% in sphere output radiance at a wavelength of 1000 nm.

7 Other Applications

The FRMS has a very low noise level and credible stability. In addition to its initial usage, it can also be used in other applications to further characterize integrating sphere sources.

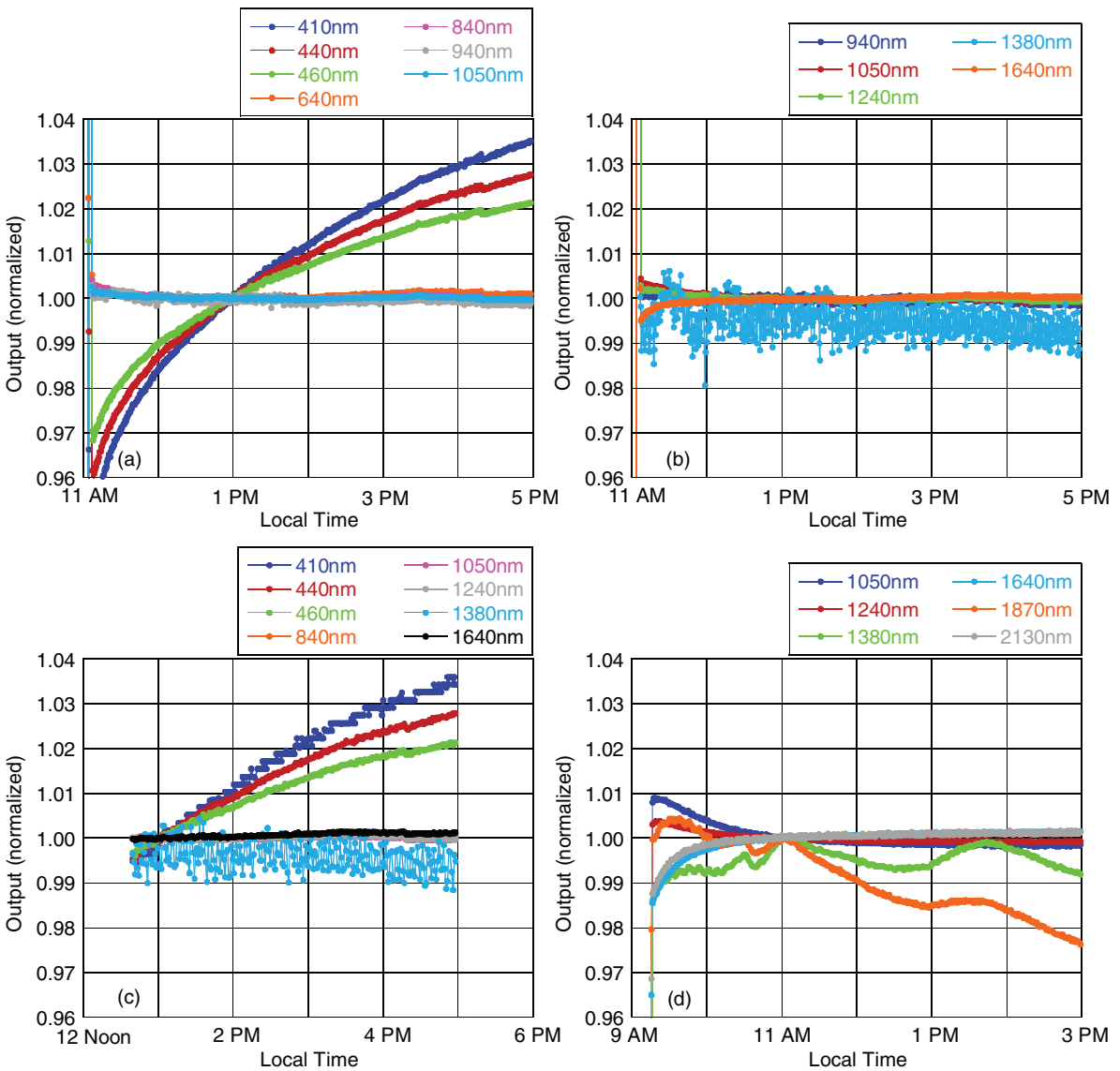

Fig. 6 Measurements of the short-term stability of the RCL 1/GSFC 1.83-m diameter Hardy sphere: (a) FRMS with Si detector, 410 to 1050 nm; (b) FRMS with InGaAs detector, 940 to 1640 nm; (c) ASD FieldSpec3 Radiometer, 410 to 1640 nm; (d) FRMS with extended InGaAs detector, 1050 to 2130 nm.

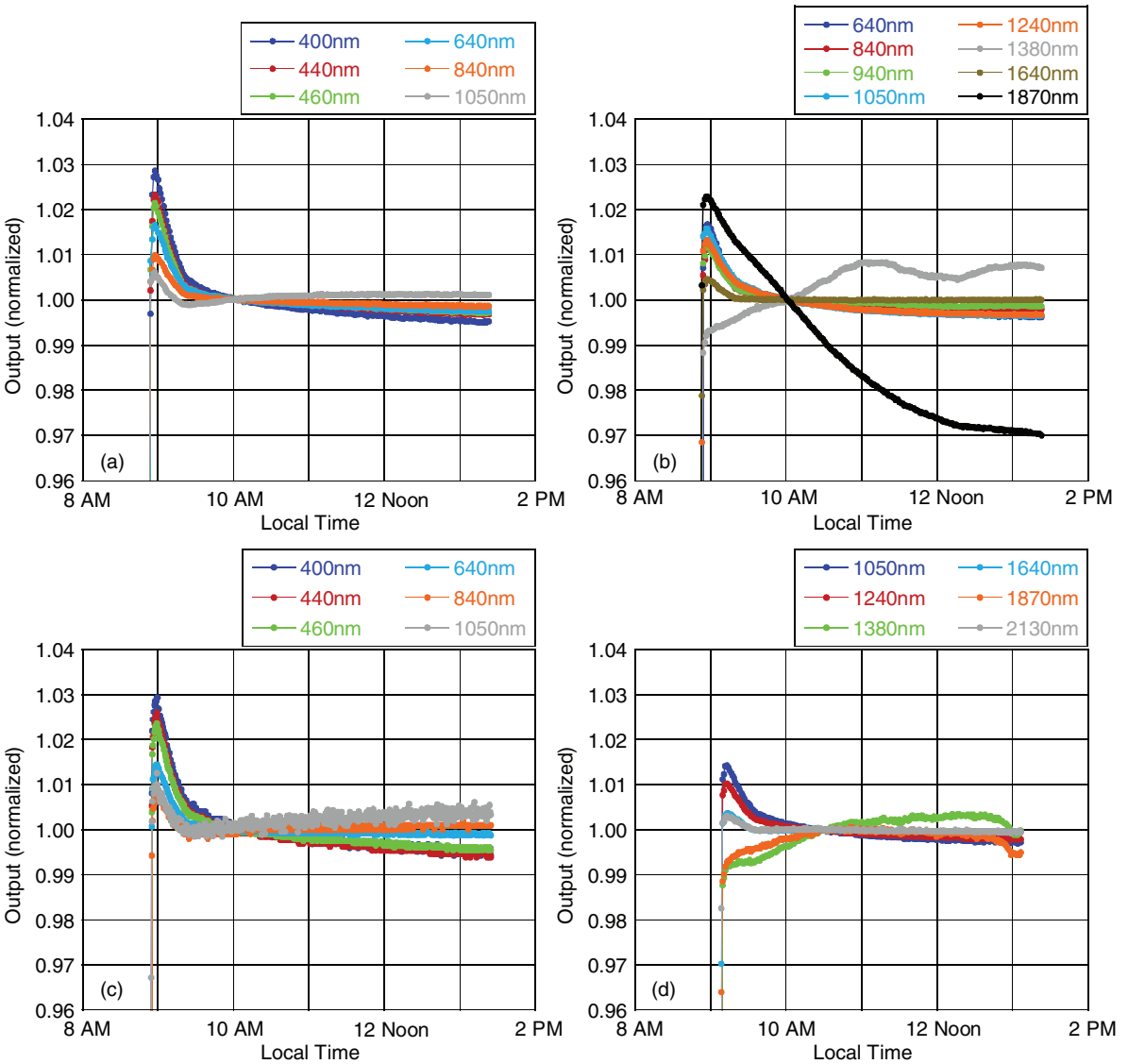

Fig. 7 Measurements of the short-term stability of the RCL 2/GSFC 91.4-cm diameter Slick sphere: (a) FRMS with Si detector, 410 to 1050 nm; (b) FRMS with Ge detector, 640 to 1870 nm; (c) Avantes spectrometer, 400 to 1050 nm; (d) FRMS with extended InGaAs detector, 1050 to 2130 nm.

7.1 *Source Aperture Mapper (SAM)*

The spatial uniformity of a calibration source factors directly into absolute errors in the calibration of moderate resolution and hyperspectral imaging instruments. The radiance uniformity of the source output is a critical characteristic for calibration, especially when the instrument is sensitive to radiance with a small FOV. The FRMS equipped with a small FOV aperture can be used to map the uniformity of the source output. An *X*-*Y* translation stage was refurbished and used to raster scan across a two-dimensional plane parallel to the aperture plane. The FRMS is mounted on the platform of the translation stage shown in Fig. 11. The scanning resolution is determined by the FOV of the FRMS and distance from the source output aperture to the detector in the FRMS. Since the distance is predetermined (i.e., 50 cm), the FOV of the FRMS solely controls the scanning resolution. A FOV of 1.91° is used to achieve the 1×1 cm scanning resolution.

In order to make more accurate measurements, a reference scanning method was used shown in Fig. 12. Using the center of the output aperture as the reference point R, the scanning sequence is Column1 → R → Column2 → R → Column3 → R and so forth. The measurement values at the reference point R were linearly interpolated and assigned to other scanning points as references. In this way, the relative uniformity at each scanning point was calculated against the reference point, R.

Figure 13 shows the uniformity plots of the four GSFC integrating spheres. Note that the 3/GSFC 50.8-cm diameter Venti sphere has a nonsymmetric lamp positioning around its exit aperture, and its output aperture size is relatively large compare to its body size. The Venti sphere uniformity shows a stratified pattern from the 9 o'clock position, where the 300 W lamp is located, to the 3 o'clock position, where the 75 W lamp is located.

7.2 *Polarization Sensitivity Measurement*

In support of the characterization of the National Polar-Orbiting Operational Environmental Satellite System

Table 2 FRMS noise equivalent spectral radiance, in $\times 10^{-2}$ W/m^2 sr μm, for select detectors and bands between 410 and 2130 nm with the FRMS operated in dc mode.

Wavelength (nm)	410	440	460	640	840	1050	1240	1380	1640	1870	2130
Si detector	0.45	0.82	0.94	0.99	0.83	0.57					
Ge detector					5.79	3.46	2.33	2.22	1.82		
InGaAs detector						11.5	4.74	3.81	1.27	4.67	2.95

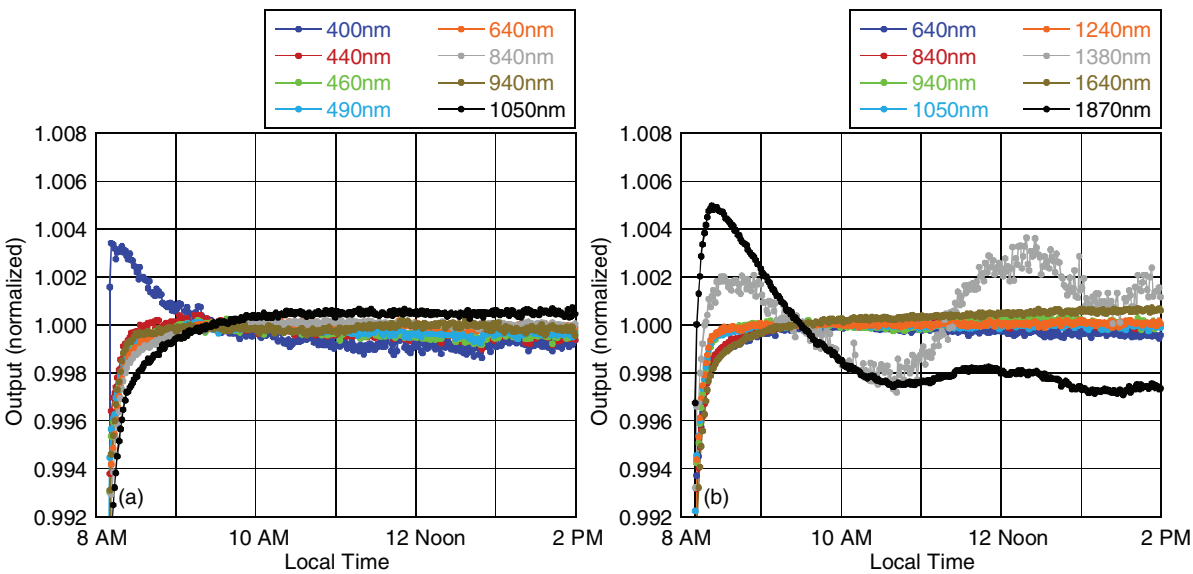

Fig. 8 Measurements of the short-term stability of the RCL 3/GSFC 50.8-cm diameter Venti sphere: (a) FRMS with Si detector, 400 to 1050 nm; (b) FRMS with Ge detector, 640 to 1870 nm.

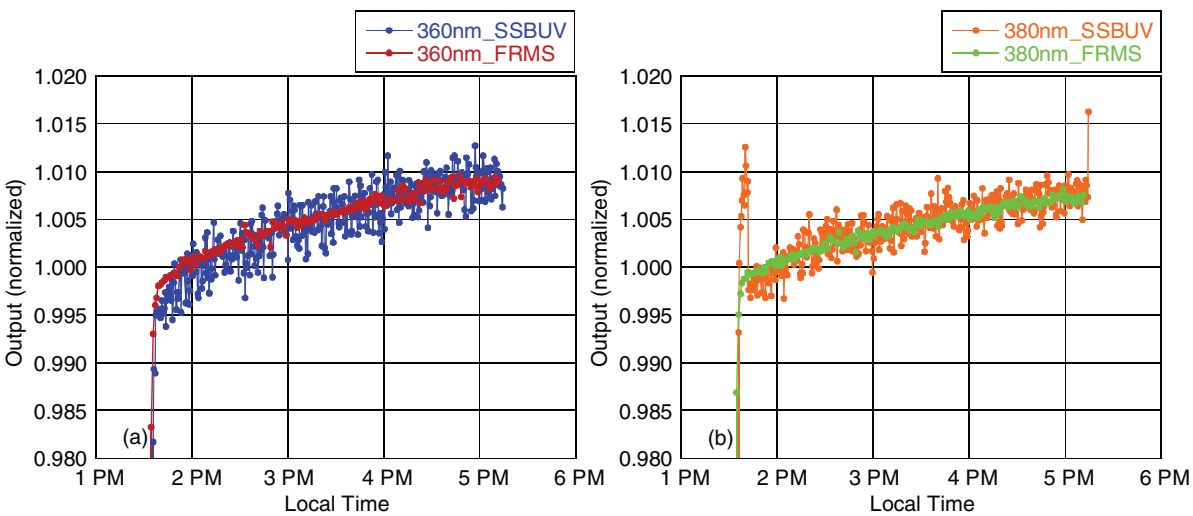

Fig. 9 FRMS and SSBUV stability measurement comparison on the 5/NASA ARC 15.2-cm diameter ARS455 sphere: (a) 360 nm; (b) 380 nm.

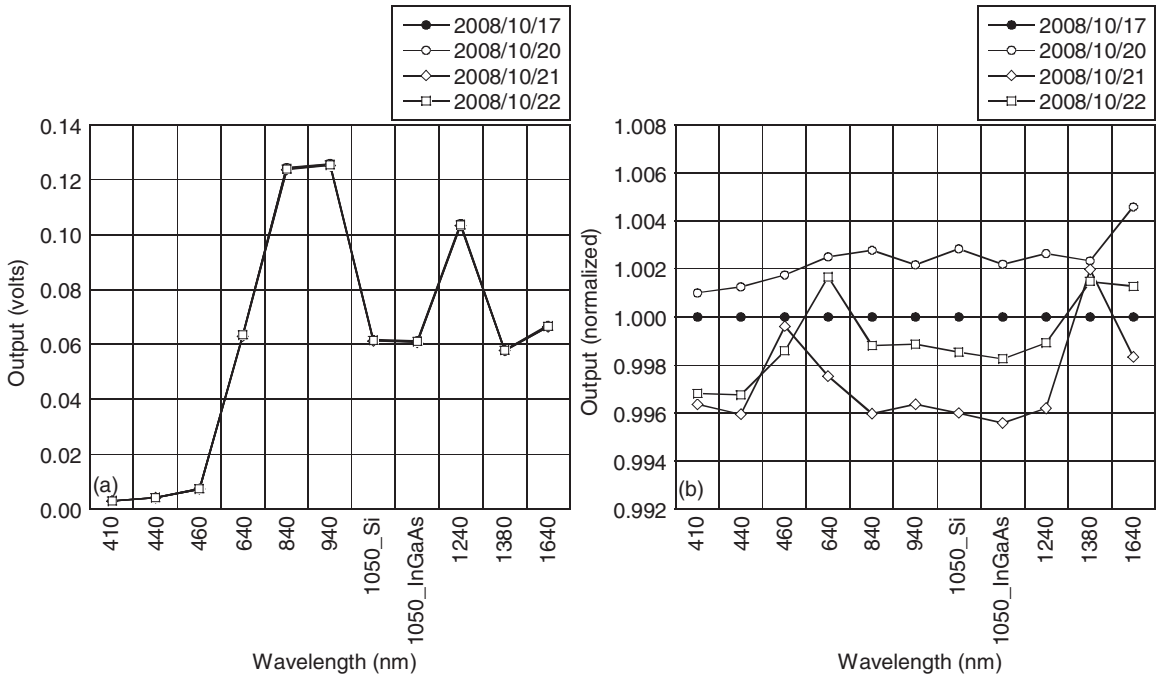

Fig. 10 Measurements of long-term stability of the RCL 1/GSFC 1.83m diameter Hardy sphere: (a) FRMS data on 4 days, 410 to 1640 nm; (b) FRMS data on 4 days normalized to October 17, 2008.

Preparatory Project (NPP) program's Visible Infrared Imager Radiometer Suite (VIIRS), preliminary polarization measurements on a flat sheet polarizer were performed using the FRMS. The measurement system set up is shown in Fig. 14. The components shown in Fig. 14 are as follows from left to right: the 30.5-cm diameter sphere source, the polarizer rotating stage, a fused silica optical flat, and the FRMS. The integrating sphere is used as a stable light source. The polarizer sheet under test is mounted on the rotating stage.

An initial baseline measurement was performed without the polarizer sheet and the optical flat. Then the polarizer was attached to the rotating stage, and the polarization component from the sphere source was measured while the polarizer was rotated. The results of this measurement indicated that the sphere source light was linearly polarized at the 0.01% to 0.001% level with the largest percentage of polarization at the shortest, 360 nm, wavelength. Finally, the optical flat was inserted and tilted 30 deg to the incident light. The resulting light intensity variations are shown in Fig. 15. The difference between these measurement data and the theoretical Fresnel prediction was less than 0.2% from 410 to 870 nm as shown in Table 3. For this calculation, the effect of multiple reflections within the optical flat was removed. The FRMS instruments have been used not only to completely characterize the polarization of RCL source outputs but also to characterize the transmittance of flat plate polarizers.

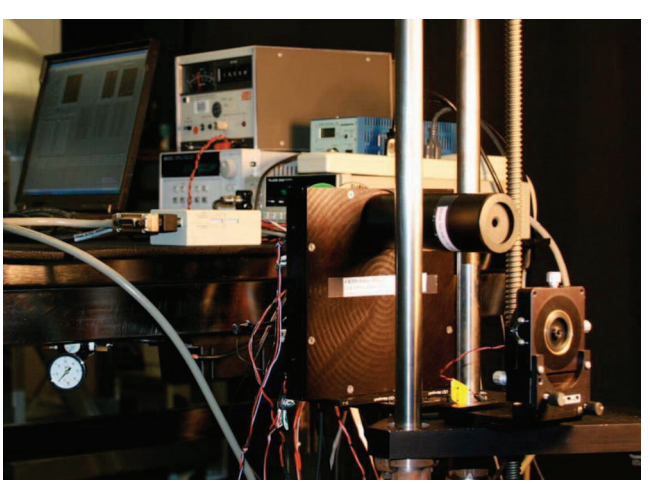

Fig. 11 The RCL SAM with FRMS as detector.

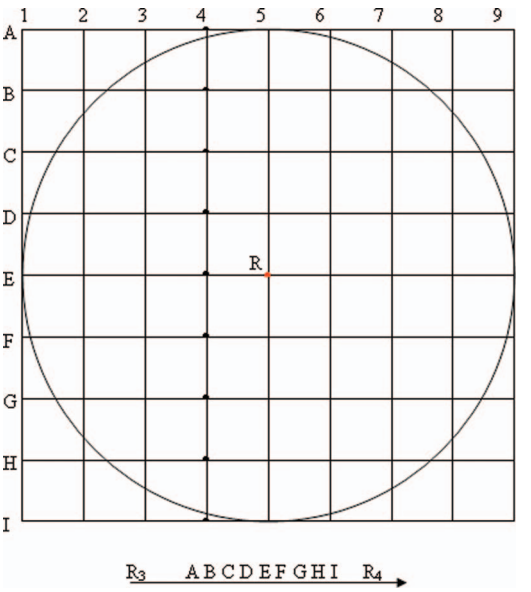

Fig. 12 The RCL SAM scanning technique.

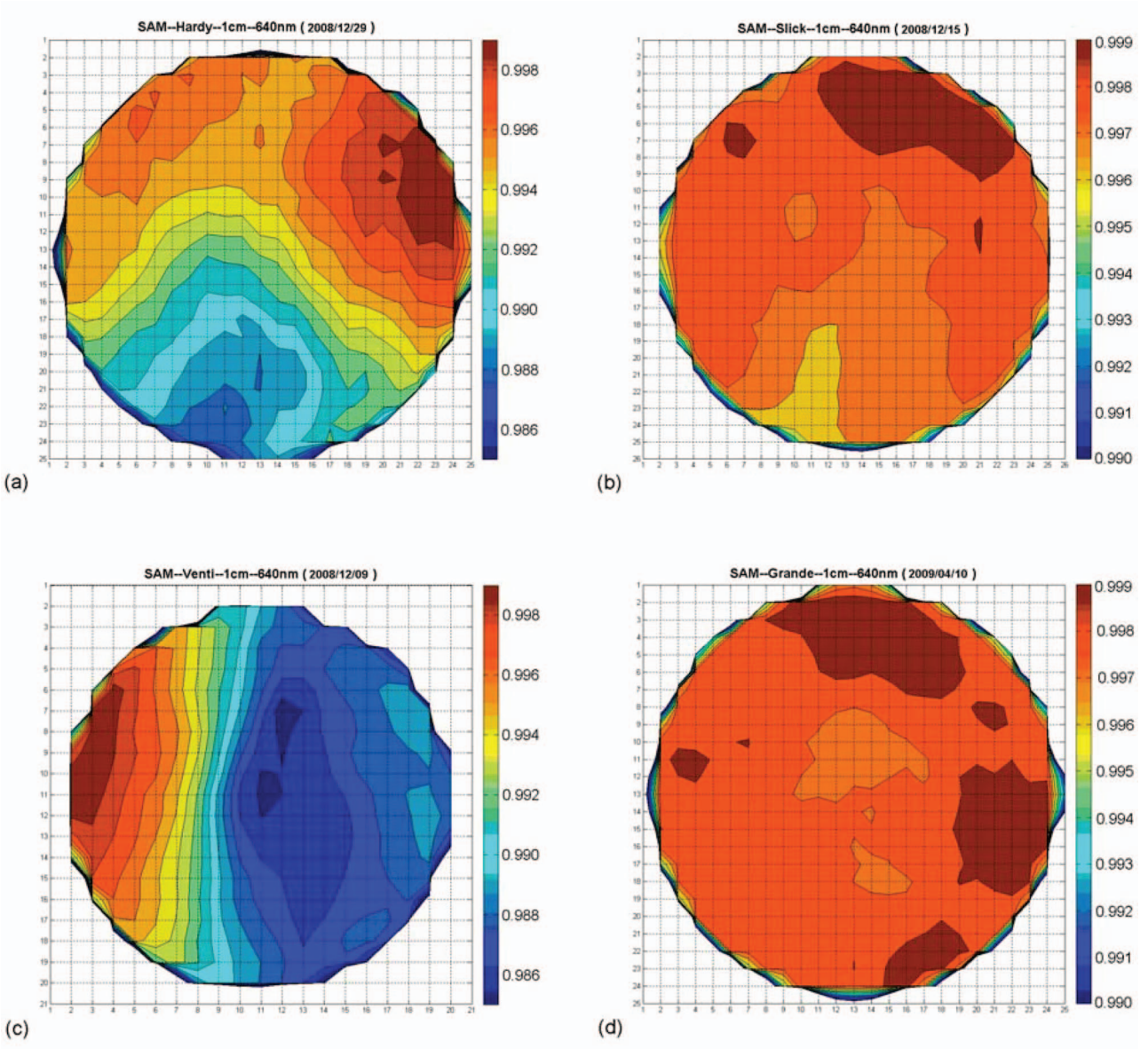

Fig. 13 FRMS SAM sphere uniformity data at 640 nm: (a) 1/GSFC 1.83-m diameter Hardy sphere; (b) 2/GSFC 91.4-cm diameter Slick sphere; (c) 3/GSFC 50.8-cm diameter Venti sphere; (d) 4/GSFC 101.6-cm diameter Grande sphere. The graduations on the *x* and *y* axes indicate centimeters.

8 Modifications for System Stability

The FRMS performs satisfactorily with Si, Ge, and standard InGaAs detectors. However, the TE cooled extended-InGaAs detector has a dark signal instability related to the environmental temperature change. Figure 16 shows the instability of the dark signal from the two-stage TE cooled extended-InGaAs detector. A reduction in the instability of the dark signal has been effected by enlarging the FOV to 6.4 deg, thereby introducing more signal. To eliminate the environmentally induced slow changes, including the temperature instability, the FRMS was modified from dc mode to ac mode using a chopper and lock-in amplifier. A chopper was added in front of the filters in the filter wheel assembly shown in Fig. 17. In this configuration, the output signal is directly sent to a lock-in amplifier for data acquisition and recording. After the modification was complete, several measurements

Table 3 Percent difference between polarization measurements using a 30 deg tilted glass plate, a flat plate polarizer, and the FRMS and the theoretical Fresnel prediction.

Wavelength (nm)	360	380	410	440	460	550	640	780	840	870	1050
Difference (%)	0.234	0.207	0.171	0.150	0.128	0.124	0.014	0.137	0.085	0.092	0.362

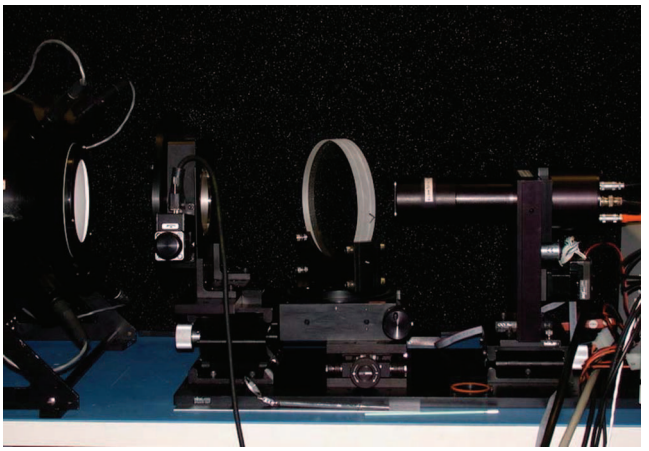

Fig. 14 Polarization measurement setup showing, from left to right, an integrating sphere, the flat sheet polarizer in a rotation stage, the glass optical flat tilted 30 deg to the primary optical axis of the setup, and the FRMS.

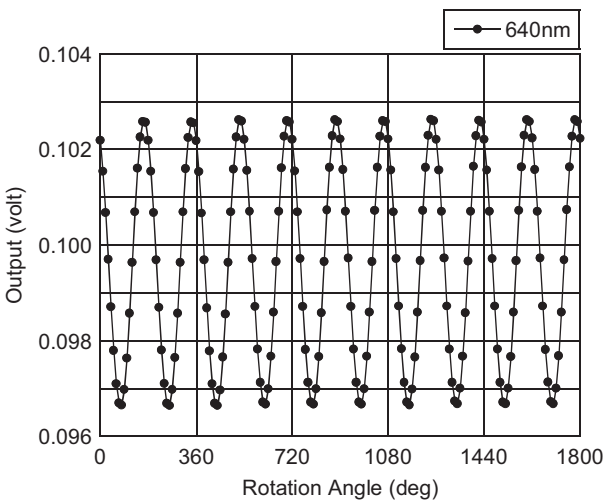

Fig. 15 FRMS signal in volts as a function of the polarization angle of the flat sheet polarizer. For these data, the FRMS viewed an integrating sphere through the sheet polarizer and a glass optical flat tilted 30 deg to the primary optical axis.

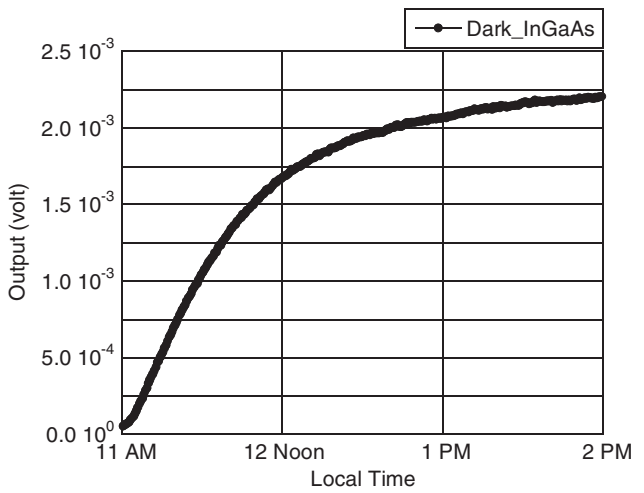

Fig. 16 Instability of the dark signal of the FRMS equipped with the thermo-electrically cooled InGaAs detector.

Fig. 17 Chopper installed before the filter wheel in the FRMS to enable ac measurements using a lock-in amplifier.

were made with an extended-InGaAs detector to compare the FRMS results in dc and ac modes. These are shown in Fig. 18.

Figure 18 contains four plots from two different lamp levels; the two plots in the upper row are from full-lamp level measurements, and the two plots in the lower row are from a lower lamp level. In these measurements, the same extended InGaAs detectors and FOV were used to provide a viable comparison. The plots show consistency in the stability trend, but they also show some differences. All the dc mode signals tend to ramp up at the beginning and drop off at the end, as compared to the ac mode. This can be explained as follows. When the 4/GSFC 101.6-cm diameter sphere "Grande" was illuminated producing more than 2 kW of additive lamp power, the room temperature gradually increased and eventually caused the dark signal of the extended InGaAs detector to increase, as shown in Fig. 16. Since the measurement results under dc mode require subtraction of the dark signal, it produced dc signals that show a higher beginning and lower end. In addition, a vertical comparison of the plots with the same wavelengths under different lamp levels indicates that, at stronger light level, the ac mode does not provide much of an advantage in the signal-to-noise performance. However, after reducing the light level, the dc mode signal gets noisier than the ac mode on the same scale. We have concluded that, under low light levels, a larger active-area detector working in the ac mode will provide better signal-to-noise performance than the dc mode.

9 Conclusions

In the absence of a stable, narrow bandpass source monitor such as the FRMS, the short- and long-term variability of integrating sphere output cannot be quantified. Without this knowledge, the sphere cannot be used as a viable calibration transfer device, since its stability and repeatability is questionable. It is the responsibility of all radiance calibration integrating sphere source users in the field to provide the use of a viable multispectral source monitor. The FRMS is singularly and uniquely qualified to serve as a stable, relatively narrow bandpass radiometer for sphere source monitoring. With reference to precision of measurement, the FRMS instrument, as a multiband filter radiometer operating in dc mode, is capable of monitoring changes in the output of

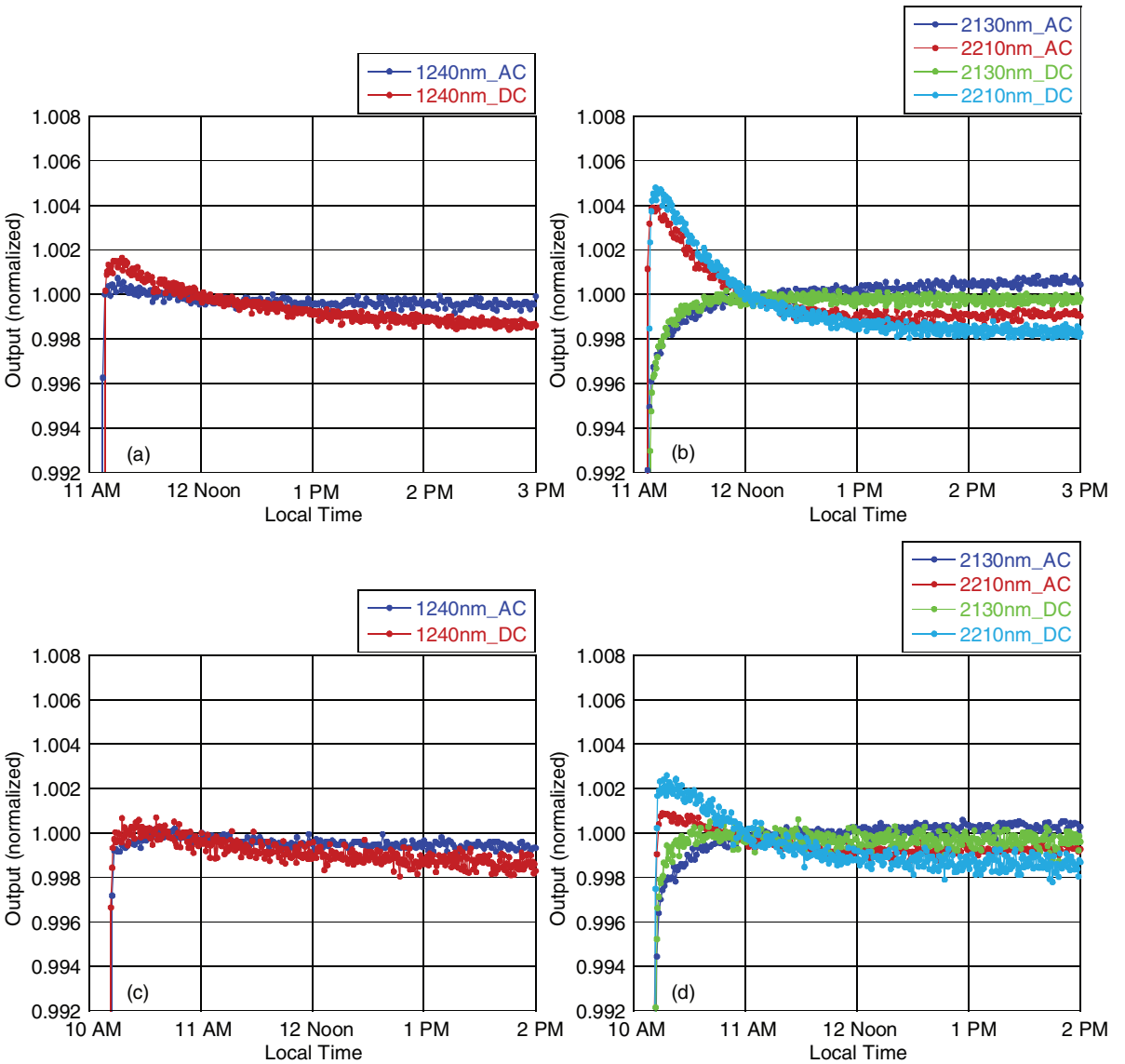

Fig. 18 Comparison of FRMS measurements made in dc and ac operating modes using the RCL 4/GSFC 101.6-cm diameter Grande sphere as a source: (a) and (b) FRMS with extended InGaAs detector viewing the sphere with eight 300 W and one 150 W lamp illuminated (i.e., full lamp level); (c) and (d) FRMS with extended InGaAs detector viewing the sphere with four 300 W lamps illuminated (i.e., lower lamp level).

integrating sphere sources at the 0.008% to 0.013% level over the 410 to 2130 nm wavelength range, excluding the 1380 nm channel which, through the sphere, is influenced by fluctuations in water vapor. The absence or presence of water vapor in the 1380 nm band does not affect the primary performance attributes of stability and precision of the FRMS. On-going FRMS data are being acquired while viewing the RCL integrating sphere sources over a period of several months in an effort to isolate and identify any long-term source degradation characteristics.

References

1. J. J. Butler, B. C. Johnson, S. W. Brown, H. W. Yoon, R. A. Barnes, B. L. Markham, S. F. Biggar, E. F. Zalewski, P. R. Spyak, J. W. Cooper, and F. Sakuma, "Radiometric measurement comparisons using transfer radiometers in support of the calibration of NASA's Earth Observing System (EOS) Sensors," *Conference on Sensors, Systems, and Next Generation Satellites V, Proc. SPIE* **3870**, 180–192 (1999).
2. J. J. Butler and R. A. Barnes, "The use of transfer radiometers in validating the visible to shortwave infrared calibrations of radiance sources used by instruments in NASA's Earth Observing System," *Metrologia* **40**, S70–S77 (2003).
3. J. J. Butler, B. C. Johnson, J. P. Rice, S. W. Brown, and R. A. Barnes, "Validation of radiometric standards for the laboratory calibration of reflected-solar Earth observing satellite instruments," in *Conference on Earth Observing Systems XII*, *Proc. SPIE* **6677**, 667707 (2007).
4. B. L. Markham, J. S. Schafer, F. M. Wood, Jr., P. W. Dabney, and J. L. Barker, "Monitoring large-aperture integrating sphere sources with a portable radiometer during satellite instrument calibration," *Metrologia* **35**, 643–648 (1998).
5. J. J. Butler, S. W. Brown, R. D. Saunders, B. C. Johnson, S. F. Biggar, E. F. Zalewski, B. L. Markham, P. N. Gracey, J. B. Young, and R. A. Barnes, "Radiometric measurement comparison on the integrating sphere source used to calibrate the Moderate Resolution Imaging Spectroradiometer (MODIS) and the Landsat 7 Enhanced Thematic Mapper Plus (ETM+)," *J. Res. Natl. Inst. Stand. Technol.* **108**, 199–228 (2003).
6. J. Marketon, P. Abel, J. J. Butler, G. R. Smith, and J. W. Cooper, "A filter radiometer monitoring system for integrating sphere sources," in *Conference on Sensors, Systems, and Next Generation Satellites*, *Proc. SPIE* **4169**, 260–267 (2001).
7. M. Johnson, *Photodetection and Measurement–Maximizing Performance in Optical Systems*, McGraw-Hill, New York, pp. 19–41 (2003).

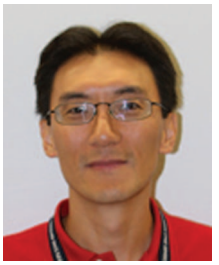

Leibo Ding studied at JiLin University in China and received his BS degree in electrical engineering in 1994. He also earned an MS degree in electrical and computer engineering at Virginia Tech in 2002. He has extensive experience in the area of radiometric calibration and characterization of satellite remote sensing instrumentation, advanced calibration methodology, and system research and development. He is currently working for Sigma Space Corporation as an instrument scientist at the NASA Goddard Space Flight Center Radiometric Calibration Laboratory.

Matthew G. Kowalewski earned his MS degree in physics at The Johns Hopkins University. He has worked in the field of remote sensing instrumentation design and calibration since 1996. He currently works for the Universities Space Research Association as a research engineer leading the technical efforts at NASA Goddard's Radiometric Calibration and Development Laboratory. His current research interests include advanced instrument component development and characterization, systems integration, radiometric calibration, and LIDAR development.

John W. Cooper is an engineer at Sigma Space Corporation, working in the Biospheric Sciences Branch at NASA's Goddard Space Flight Center. He has over 22 years of experience in the field of radiometric calibration and characterization. He specializes in characterization and operation of spherical integrating radiometric sources, irradiance lamp standards, and spectrometers. During the 1990s he contributed to the calibration, operation, and documentation of high-altitude underflights for vicarious calibrations of on-orbit satellite platforms. Throughout his career he contributed to projects involving characterization and validation of satellite, aircraft, and ground instrumentation, and participated in field missions and conferences in the U.S. and abroad, including Canada, Brazil, Portugal, China, and Japan. He participates in intercalibration field projects with several universities, instrument manufacturers, and government agencies.

Gilbert R. Smith studied at the Baltimore Polytechnic Institute where he received his diploma in electrical engineering in 1948. He began work at the Johns Hopkins University Physics Department as an assistant to experimental physicist John D. Strong and to his graduate students in the conduct of infrared basic research and high vacuum technology. He also attended McCoy College, the Johns Hopkins University night school, for an extended period in graduate studies. In 1961, at the Westinghouse Electric Applied Research Division, he was responsible for the design and fabrication of the Thermicon Infrared Retina. He became a registered professional electrical engineer in 1967. Concurrently, he began work with NOAA NESDIS at the NASA Goddard Space Flight Center as an aerospace engineer with responsibility for instrument design, fabrication, testing, and calibration for several NOAA and NASA satellite programs. In the early 1980s he worked with Warren Hovis on pre-launch satellite instrument calibration and on post-launch vicarious calibration using high altitude aircraft. From 1987 to 1989, he was chief of the Experimental Applications Branch at NOAA NESDIS. Currently, he is retired and working for Sigma Space Corporation as a consultant in the Radiation Calibration Laboratory at NASA Goddard Space Flight Center. He is a member of OSA.

Robert A. Barnes received BS and PhD degrees in analytical chemistry from Drexel University in Philadelphia, Pennsylvania. From 1979 to 1991, he was a research scientist for Chemal, Inc. at NASA's Wallops Flight Facility, providing rocket- and balloon-based measurements of stratospheric ozone and temperature for satellite instrument validation. Since 1991, he has been employed by the Sciences Applications International Corporation at NASA's Goddard Space Flight Center as a satellite instrument calibration scientist. Those instruments have included SeaWiFS, VIRS on TRMM, MODIS on Terra, and OLI on LDCM. In addition, he has worked for the EOS calibration program and on SIMBIOS, a project that combined measurements from different satellite instruments into a unified ocean color data set. Currently, he works on the NPP calibration program and on the calibration of NPP VIIRS, plus the development of new calibration techniques for the next-generation of NASA Earth-observing satellites.

Eugene Waluschka received a PhD in physics in 1975 from the New York University. In 1976, he joined the Mathematical Applications Group located in Elmsford, New York working in the areas of nuclear radiation transport by Monte Carlo methods, simulation of aircraft laser signatures, and computer graphics. In 1980 joined the Perkin-Elmer Corporation (now Goodrich) in Connecticut, spending most of his time modeling and numerically simulating various phenomena. Currently, he is a member of the optics group at NASA's Goddard Space Flight Center providing technical support to various programs.

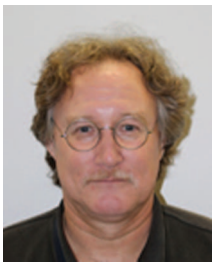

James J. Butler is an optical physicist in the Biospheric Sciences Branch at NASA's Goddard Space Flight Center. He has served as EOS calibration scientist since 1995 and deputy NPP project scientist for Instruments and Calibration since 2004. He also serves as the principal investigator of NASA's Radiometric and Diffuser Calibration Laboratories. His primary areas of active research include the calibration and characterization of remote sensing instrumentation and optical metrology. His previous research experience at NASA includes ground-based and balloon-borne lidar for the detection of stratospheric molecular and radical species and laser-induced fluorescence of molecules and radicals. As a research associate at NIST, he conducted research in the photoionization and dissociation dynamics of state selected hydrocarbons and in photoelectron spectroscopy. He received a BS degree in physical chemistry from the University of Notre Dame in 1977 and a PhD degree in physical chemistry from the University of North Carolina.